



Two Jovian Planets around the Giant Star HD 202696: A Growing Population of Packed Massive Planetary Pairs around Massive Stars?

Trifon Trifonov¹ , Stephan Stock² , Thomas Henning¹ , Sabine Reffert² , Martin Kürster¹ , Man Hoi Lee^{3,4} ,
Bertram Bitsch¹ , R. Paul Butler⁵ , and Steven S. Vogt⁶

¹ Max-Planck-Institut für Astronomie, Königstuhl 17, D-69117 Heidelberg, Germany; trifonov@mpia.de

² Landessternwarte, Zentrum für Astronomie der Universität Heidelberg, Königstuhl 12, D-69117 Heidelberg, Germany

³ Department of Earth Sciences, The University of Hong Kong, Pokfulam Road, Hong Kong

⁴ Department of Physics, The University of Hong Kong, Pokfulam Road, Hong Kong

⁵ Department of Terrestrial Magnetism, Carnegie Institution for Science, Washington, DC 20015, USA

⁶ UCO/Lick Observatory, Department of Astronomy and Astrophysics, University of California at Santa Cruz, Santa Cruz, CA 95064, USA

Received 2018 September 24; revised 2018 December 18; accepted 2018 December 18; published 2019 February 4

Abstract

We present evidence for a new two-planet system around the giant star HD 202696 (=HIP 105056, BD +26 4118). The discovery is based on public HIRES radial velocity (RV) measurements taken at Keck Observatory between 2007 July and 2014 September. We estimate a stellar mass of $1.91_{-0.14}^{+0.09} M_{\odot}$ for HD 202696, which is located close to the base of the red giant branch. A two-planet self-consistent dynamical modeling MCMC scheme of the RV data followed by a long-term stability test suggests planetary orbital periods of $P_b = 517.8_{-3.9}^{+8.9}$ and $P_c = 946.6_{-20.9}^{+20.7}$ days, eccentricities of $e_b = 0.011_{-0.011}^{+0.078}$ and $e_c = 0.028_{-0.012}^{+0.065}$, and minimum dynamical masses of $m_b = 2.00_{-0.10}^{+0.22}$ and $m_c = 1.86_{-0.23}^{+0.18} M_{\text{Jup}}$, respectively. Our stable MCMC samples are consistent with orbital configurations predominantly in a mean period ratio of 11:6 and its close-by high-order mean-motion commensurabilities with low eccentricities. For the majority of the stable configurations, we find an aligned or anti-aligned apsidal libration (i.e., $\Delta\omega$ librating around 0° or 180°), suggesting that the HD 202696 system is likely dominated by secular perturbations near the high-order 11:6 mean-motion resonance. The HD 202696 system is yet another Jovian-mass pair around an intermediate-mass star with a period ratio below the 2:1 mean-motion resonance. Therefore, the HD 202696 system is an important discovery that may shed light on the primordial disk–planet properties needed for giant planets to break the strong 2:1 mean-motion resonance and settle in more compact orbits.

Key words: planetary systems – planets and satellites: detection – planets and satellites: dynamical evolution and stability – techniques: radial velocities

1. Introduction

By 2018 November, 647 known multiple-planet systems were reported in the literature,⁷ 144 of which were discovered using high-precision radial velocity (RV) measurements. The RV technique is very successful in determining the orbital architectures of multiple extrasolar planetary systems. In some exceptional cases, N -body modeling of precise Doppler data in resonant or near-resonant multiple systems can reveal the system’s dynamical properties and constrain the planets’ true dynamical masses and mutual inclinations (e.g., Rivera et al. 2010; Tan et al. 2013; Trifonov et al. 2014, 2018; Nelson et al. 2016 and references therein). Therefore, multiple-planet systems discovered with the Doppler method are fundamentally important in order to understand planet formation and evolution in general.

After publication of the Keck HIRES (Vogt et al. 1994) velocity archive by Butler et al. (2017), it became apparent that the early K giant star HD 202696 most likely hosts another RV multiplanet system. The HIRES data set comprises 42 precise RVs of HD 202696 taken between 2007 July and 2014 September, which we find to be consistent with at least two planets in the Jovian-mass regime with periods of ~ 520 days for the inner planet and ~ 950 days for the outer planet. The HD 202696 system is remarkable because of the small orbital separation between the two massive planets forming an orbital period ratio close to the 9:5

mean-motion resonance (MMR). Notable examples of small-separation pairs around intermediate-mass stars are 24 Sex, η Ceti, and HD 47366 (between 9:5 and 2:1 MMR; Johnson et al. 2011; Trifonov et al. 2014; Sato et al. 2016); HD 200964 and HD 5319 (4:3 MMR; Johnson et al. 2011; Giguere et al. 2015); and HD 33844 (5:3 MMR; Wittenmyer et al. 2016). These systems may indicate that more massive stars tend to form more massive planetary systems, a fraction of which pass the strong 2:1 MMR during the inward planet migration phase and settle at high-order resonant or near-resonant configurations with period ratios $< 2:1$. The dynamical characterization of the relatively compact system around HD 202696 may help to enhance our understanding of the formation of massive multiple-planet systems around intermediate-mass stars.

This paper is organized as follows. In Section 2, we present our estimates of the stellar properties of HD 202696. Section 3 presents our Keplerian and N -body dynamical RV modeling analysis, which reveals the planets HD 202696 b and c. In Section 4, we present the long-term stability analysis of the HD 202696 system and its dynamical properties. In Section 5, we provide a brief discussion of the HD 202696 system in the context of current knowledge of compact multiple-planet systems around giant stars. Finally, Section 6 provides a summary of our results.

2. Stellar Parameter Estimates of HD 202696

The giant star HD 202696 (=HIP 105056, BD +26 4118) is a bright $V = 8.2$ mag star of spectral class K0III/IV with

⁷ <http://exoplanet.eu>

$B - V = 1.003$ mag (ESA 1997). The second *Gaia* data release (*Gaia* DR2; Gaia Collaboration et al. 2016, 2018) lists a parallax of $\pi = 5.28 \pm 0.04$ mas, an effective temperature $T_{\text{eff}} = 4951.4$ K, a radius estimate of $6.01 R_{\odot}$, and a mean $G = 7.96$ mag. Bailer-Jones et al. (2018) carried out a Bayesian inference using the DR2 parallax information with a prior on distance and estimated a distance of $188.5^{+1.6}_{-1.6}$ pc.

For the dynamical analysis of the HD 202696 system, we need to incorporate the stellar parameters of the host star, most importantly its stellar mass. This is achieved by applying a slightly modified version of the methodology and Bayesian inference scheme used in Stock et al. (2018), which was particularly optimized for subgiant and giant stars such as HD 202696 and is capable of determining the post-main-sequence evolutionary stage. The method was shown to provide robust estimates of stellar parameters such as mass M , radius R , age τ , effective temperature T_{eff} , surface gravity $\log g$, and luminosity L in agreement with other methods, such as asteroseismology, spectroscopy, and interferometry. The method uses the trigonometric parallax, a metallicity estimate, and photometry in at least two different bands as input parameters. We decided to use the *Hipparcos* V and B photometry as in Stock et al. (2018) instead of the available high-precision *Gaia* DR2 photometry because it was shown that results based on this choice of photometry are in good agreement with literature values. While *Gaia* DR2 photometry is more precise, it has yet to be tested whether comparisons with stellar evolutionary models suffer from systematics, which is especially important regarding the small photometric uncertainties. Stock et al. (2018) adopted the stellar models based on the PAdova and TRieste Stellar Evolution Code (PARSEC; Bressan et al. 2012) and used bolometric corrections by Worthey & Lee (2011). The Bayesian inference is normally carried out in the plane of the astrometric-HR diagram (Arenou & Luri 1999), which has a color as the abscissa and the astrometry-based luminosity (ABL) in a specific photometric band λ as the ordinate. The ABL is a quantity that is linear in the trigonometric parallax, allowing for unbiased comparisons of stellar positions to evolutionary models if the parallax error dominates. However, HD 202696 is affected by a significant amount of extinction, which, in addition, is very uncertain. Gontcharov & Mosenkov (2018) estimated a reddening of $E(B - V) = 0.08$ mag and an extinction of $A_V = 0.25$ mag in the V band for HD 202696. They also stated that their reddening estimates are better than 0.04 mag, a value that we conservatively adopt as the formal reddening error for HD 202696. We used the python spectral energy distribution (SED) fitting tool by Robitaille et al. (2007) together with the model atmospheres of Castelli & Kurucz (2004) to fit the available broadband photometry of HD 202696. We derived an extinction of $A_V = 0.144^{+0.280}_{-0.012}$ mag, consistent with the value and uncertainties by Gontcharov & Mosenkov (2018). However, due to the sparse sampling of the model atmospheres, the errors of the SED fitting are probably underestimated and should be regarded with caution. For the analysis of the stellar parameters in this paper, we used the extinction by Gontcharov & Mosenkov (2018). As the uncertainty of the extinction is the dominating factor in the determination of the stellar parameters of HD 202696, it is justified to use the absolute magnitude of the star instead of the ABL for the determination of stellar parameters and include the uncertainties of the extinction. We use the Bayesian distance estimate by Bailer-Jones et al. (2018) for the determination of the absolute magnitude from the distance modulus. This decreases biases that arise when determining the

Table 1
Stellar Parameters of HD 202696 and Their 1σ Uncertainties

Parameter	HD 202696	Reference
Spectral type	K0III-IV	[1]
V [mag]	8.23 ± 0.01	[1]
$B - V$ [mag]	1.003 ± 0.005	[1]
$E(B - V)$ [mag]	0.08 ± 0.04	[2]
A_V [mag]	0.25 ± 0.13	[2]
π [mas]	5.28 ± 0.04	[3]
RV_{absolute} [km s $^{-1}$]	-34.45 ± 0.22	[3]
Radius [R_{\odot}]	$6.01^{+0.33}_{-0.19}$	[3]
T_{eff} [K]	4951^{+78}_{-129}	[3]
Distance [pc]	$188.5^{+1.6}_{-1.6}$	[4]
From Bayesian inference ^a		
Mass [M_{\odot}]	$1.91^{+0.09}_{-0.14}$	This paper
Radius [R_{\odot}]	$6.43^{+0.41}_{-0.39}$	This paper
Luminosity [L_{\odot}]	$23.4^{+2.4}_{-2.0}$	This paper
Age [Gyr]	$1.32^{+0.35}_{-0.25}$	This paper
T_{eff} [K]	5040^{+71}_{-85}	This paper
$\log g$ [cm s $^{-2}$]	$3.11^{+0.07}_{-0.07}$	This paper
Evolutionary stage	RGB ($P = 0.996$)	This paper
Evolutionary phase ^b	$8.30^{+0.13}_{-0.11}$	This paper
From spectra ^c		
T_{eff} [K]	4988 ± 57	This paper
$\log g$ [cm s $^{-2}$]	3.24 ± 0.15	This paper
[Fe/H]	0.02 ± 0.04	This paper
$v \cdot \sin(i)$ [km s $^{-1}$]	2.0 ± 0.8	This paper
RV_{absolute} [km s $^{-1}$]	-33.17 ± 0.05	This paper

Notes.

^a Following Stock et al. (2018).

^b A value of 8.0 marks the red giant base, while 9.0 marks the red giant branch bump (Bressan et al. 2012).

^c From HIRES spectra using CERES (Brahm et al. 2017a) and ZASPE (Brahm et al. 2017b).

References. [1] ESA (1997), [2] Gontcharov & Mosenkov (2018), [3] Gaia Collaboration et al. (2016, 2018), [4] Bailer-Jones et al. (2018).

absolute magnitude from the trigonometric parallax, which is why the ABL should normally be the preferred quantity.

We need to determine the spectroscopic metallicity of HD 202696 in order to derive the stellar mass. We derive spectroscopic stellar parameters such as T_{eff} , surface gravity $\log g$, metallicity [Fe/H], and $v \cdot \sin(i)$ by using the available HIRES spectral observations of HD 202696. As the spectra obtained at Keck Observatory have severe iodine (I_2) line contamination imposed in order to measure RVs using the I_2 method (Marcy & Butler 1992; Valenti et al. 1995; Butler et al. 1996), we use the single I_2 -free stellar template spectrum⁸ required for the RV modeling process (see Butler et al. 1996) to determine our spectroscopic parameters. We reduce the I_2 -free spectrum, with a signal-to-noise ratio of approximately 120, using the CERES pipeline (Brahm et al. 2017a) and then analyze it by using ZASPE (Brahm et al. 2017b). Table 1 provides our spectral stellar parameter estimates of HD 202696.

Using the spectroscopic metallicity estimate, the B and V photometry of the *Hipparcos* catalog, and the Bayesian distance estimate of Bailer-Jones et al. (2018), together with their uncertainties, we apply the slightly modified Bayesian inference method of Stock et al. (2018) and determine that HD 202696 is,

⁸ Downloaded from <http://nexsci.caltech.edu/archives/koa/>.

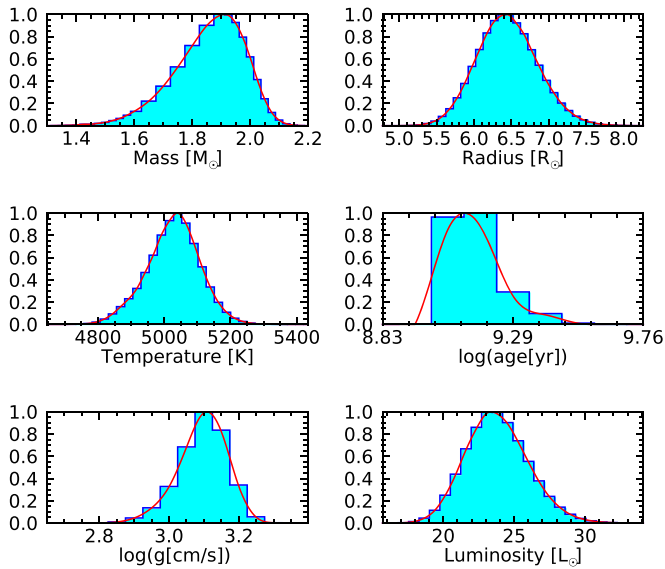


Figure 1. Bayesian stellar parameters estimated using the *Gaia* DR2 parallax, *Hipparcos* *B* and *V* photometry, and the spectroscopic metallicity.

with a probability of 99.6%, an early red giant branch star right at the beginning of its ascent. We neglect the small probability of the star belonging to the horizontal branch. We estimate a stellar mass of $M = 1.91_{-0.14}^{+0.09} M_{\odot}$, a luminosity of $L = 23.4_{-2.4}^{+2.0} L_{\odot}$, and an age of $1.32_{-0.25}^{+0.35}$ Gyr. The derived effective temperature of $T_{\text{eff}} = 5040_{-85}^{+71}$ K is within 1σ of our spectroscopic estimate (4988 ± 57 K) and the estimate by *Gaia* DR2 (4951_{-129}^{+78} K). The same is true for the surface gravity of $\log g = 3.11_{-0.07}^{+0.07}$ dex when compared to our spectroscopic estimate (3.24 ± 0.15 dex) and the radius $R = 6.43_{-0.39}^{+0.41} R_{\odot}$ when compared to the *Gaia* DR2 estimate ($6.01_{-0.19}^{+0.33} R_{\odot}$). Given the Bayesian stellar radius and the $v \cdot \sin(i) = 2.0 \pm 0.8$ km s $^{-1}$ estimated from the spectra, we calculate a stellar rotational period of $P_{\text{rot}} = 162.7 \pm 65.9$ days, which is typical for an early evolved star such as HD 202696.

The good agreement between the Bayesian stellar parameters and the other estimates strengthens our confidence in the adopted extinction of the star, as the extinction is significant and our results rather sensitive to the precise extinction value. Neglecting extinction, the resulting mass would have been $\sim 1.4 M_{\odot}$, considerably smaller than before, and the stellar parameters would not have been consistent with constraints provided by spectroscopy and *Gaia* DR2 data. However, the fact that extinction and reddening are consistent with zero at the 2σ level leads to a relatively large uncertainty of the stellar mass, especially toward lower masses. The posterior distribution for each of the stellar parameters determined from the Bayesian inference is shown in Figure 1, while Figure 2 shows the Padova evolutionary tracks in the color–magnitude diagram (CMD) for various initial stellar masses and the CMD position of HD 202696. The Bayesian stellar parameters, which were determined from the maximum of the distribution, along with their 1σ error estimates, are summarized in Table 1.

3. Analysis of RV Data Set

3.1. Period Search

The HIRES RV time series of HD 202696 consists of 42 precise Doppler measurements taken between 2007 July and 2014 September. With a median RV precision of 1.37 m s $^{-1}$

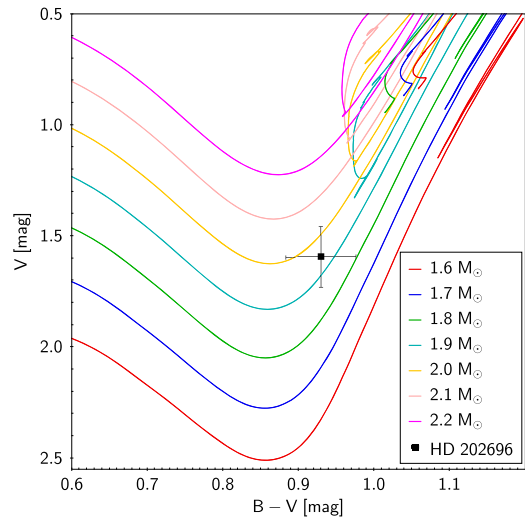


Figure 2. Padova evolutionary tracks of metallicity $Z = 0.015875$ ($[\text{Fe}/\text{H}] \approx 0.02$) with various initial stellar masses from 1.6 (red line) to 2.2 (pink line) M_{\odot} in steps of $0.1 M_{\odot}$ in the CMD. The position of HD 202696 is highlighted as the black point.

and an end-to-end amplitude of 127 m s $^{-1}$, these data clearly show systematic motions, resembling two Keplerians caused by two massive orbiting planets. Figure 3 shows the precise RV data of HD 202696, together with our best two-planet Keplerian model and its uncertainties, while Figure 4 shows the two fairly well-sampled Keplerian signals phase-folded at their best-fit periods (see Section 3.2 for a quantitative analysis of the data). Note that the data uncertainties displayed in Figures 3 and 4 already contain the best-fit RV jitter estimate of ~ 8 m s $^{-1}$, which was automatically added in quadrature to the error budget during the fitting. This RV jitter estimate is typical for early K giants such as HD 202696 and is likely due to solar-like oscillations, which have periods of less than a day and are thus not resolved in the long-term RV time series. The scaling relations from Kjeldsen & Bedding (2011) predict 3.7 m s $^{-1}$ RV jitter for HD 202696, while the typical RV jitter value for a star with a $B - V$ color of 1.003 mag in the Lick sample is 10 – 20 m s $^{-1}$ (see Figure 3 in Trifonov et al. 2014). Since the stars in the Lick sample are, on average, slightly more evolved than HD 202696, it might be reasonable to expect HD 202696 to have slightly smaller RV jitter than most other stars in this sample.

It is worth noting that with the release of the HIRES database, Butler et al. (2017) reported the presence of at least three periods in the Keck data of HD 202696. They identified two significant signals with periods of 522.3 ± 6.4 and 946.0 ± 19.0 days, classified as planetary “candidates,” and an additional period of 214.2 ± 4.8 days, which required further confirmation.

As an independent test, we derive the generalized Lomb–Scargle periodogram (GLS; Zechmeister & Kürster 2009) of the HIRES RV data, as well as that of the S- and H-index activity indicators (Figure 5) also provided by Butler et al. (2017). These time series are tabulated in Table 2. For reference, in all panels of Figure 5, the range of possible stellar rotation frequencies of HD 202696 is indicated by the red shaded area, with the red dashed line at the most likely value ($1/P_{\text{rot}} = 0.00615_{-0.00177}^{+0.00418}$ day $^{-1}$; see Section 2). The horizontal dotted, dot-dashed, and dashed lines correspond to false-alarm probability (FAP) levels of 10%, 1%, and 0.1%, respectively.

We use an FAP $< 0.1\%$ as our significance threshold. The top panel of Figure 5 reveals a dominant signal around 540 days (blue dashed line) in the HIRES RVs, which is significant. The second panel of Figure 5 shows the periodogram of the RV data after the ~ 540 day signal has been subtracted; it indicates a second significant signal with a period of ~ 970 days (green dashed line). The middle panel of Figure 5 shows that no period with an FAP $< 0.1\%$ can be detected after the two most significant signals have been consecutively subtracted from the data.

The ~ 214 day signal previously reported by Butler et al. (2017) is also visible in the residuals of the data, but with $1\% < \text{FAP} < 10\%$, which we consider insignificant. Moreover, the 214 day signal falls within the red shaded area of possible stellar rotation frequencies and thus is not considered further in our analysis. No significant periodicities can be identified in the two panels of Figure 5, which show the periodograms of the H- and S-index activity indicators, respectively.

Additionally, we inspected the V-band measurements of HD 202696 from the All-Sky Automated Survey (ASAS; Pojmanski et al. 2005). We find only 48 high-quality ASAS V-band measurements (graded A and B with $\overline{\sigma_V} = 0.037$ mag), mostly taken between 2003 May and 2007 October, i.e., prior to the HIRES Doppler observations of HD 202696. Thus, the sparse ASAS photometry is only relevant to check for evident intrinsic photometric variability, which could be associated with the RV signals. No significant periodicity is observed in any of the five available ASAS apertures. The bottom panel of Figure 5 shows the GLS periodogram of the averaged ASAS photometry measurements, indicating that HD 202696 is most likely a photometrically stable star.

The two significant signals at ~ 540 and ~ 970 days are consistent with those reported by Butler et al. (2017) as planet candidates. We find that these signals are not consistent with the range of possible stellar rotation frequencies of HD 202696. Also, the S- and H-index activity indicators of the HIRES data and ASAS photometry do not show any significant periodic structure or correlation that could be associated with the RV signals. Thus, we consider the ~ 540 and ~ 970 day signals as robust planetary detections.

3.2. Orbital Parameter Estimates

In order to determine the orbital parameters of the HD 202696 b and c planetary companions, we adopt a maximum-likelihood estimator (MLE) scheme coupled with a Nelder–Mead algorithm (also known as a downhill simplex algorithm; see Nelder & Mead 1965; Press et al. 1992). In our scheme, we minimize the negative logarithm of the model’s likelihood function ($-\ln \mathcal{L}$), while we simultaneously optimize the planetary RV semi-amplitudes $K_{b,c}$, periods $P_{b,c}$, eccentricities $e_{b,c}$, arguments of periastron $\omega_{b,c}$, mean anomalies $M_{b,c}$, and the RV zero-point offset. Prior information on the period, phase, and amplitude for each of the two-planet candidates is taken from the GLS periodogram test (see Figure 5), which provides good starting parameters for the MLE algorithm. All parameters are derived for a uniform reference epoch of 2,450,000 (BJD). Following Baluev (2009), we also include the RV jitter⁹ as an additional parameter in the modeling.

⁹ The RV jitter is most likely due to a combination of astrophysical stellar noise and possible instrument and data reduction systematics.

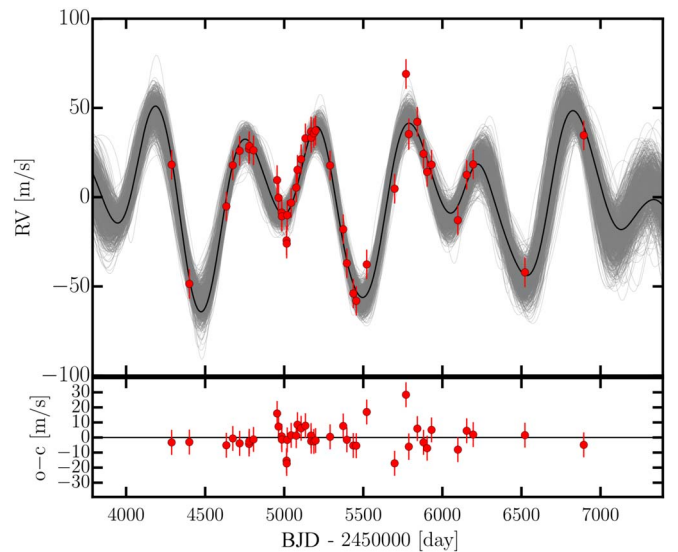


Figure 3. The top panel shows the available precise RV data of HD 202696 measured with HIRES between 2007 July and 2014 September. The solid curve is the best two-planet Keplerian model fitted to the data, while the shaded area is composed of 1000 randomly chosen confident fits from an MCMC test constructed to study the parameter distribution. The bottom panel shows the best-fit residuals. After removing the two Keplerian components of the RV signal with semi-amplitudes of ~ 32 and 28 m s^{-1} , the RV scatter has an rms of 8.3 m s^{-1} , which is mostly consistent with the expected short-period stellar jitter for this target.

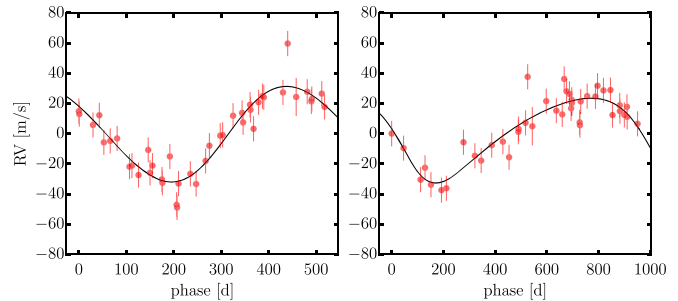


Figure 4. Two Keplerian signals with periods of 521.0 and 956.1 days, respectively, shown in a phase-folded representation.

We apply two models to the RV data: a standard unperturbed two-planet Keplerian model and a more accurate self-consistent N -body dynamical model, which models the gravitational interactions between the planets by integrating the equations of motion using the Gragg–Bulirsch–Stoer integration method (Press et al. 1992). We cross-check the obtained best-fit results for consistency with the Systemic Console 2.2 package (Meschiari et al. 2009) and find excellent agreement between our MLE code¹⁰ and Systemic.

For parameter distribution analysis and uncertainty estimates, we couple our MLE fitting algorithm with a Markov chain Monte Carlo (MCMC) sampling scheme using the emcee sampler (Foreman-Mackey et al. 2013). For all parameters, we adopt flat priors (i.e., equal probability of occurrence), and we run emcee from the best fit obtained by the MLE. We select the 68.3% confidence levels of the posterior MCMC parameter distribution as 1σ parameter uncertainties.

¹⁰ The source code and GUI of our tools can be found in <https://github.com/3fon3fonov/trifon> (T. Trifonov et al. 2018, in preparation).

The best-fit parameters of our two-planet Keplerian and dynamical models, together with their 1σ MCMC uncertainties, are tabulated in Table 3. We first fit the Keplerian model, and as a next step, we adopt the best two-planet Keplerian parameters as an input for the more sophisticated dynamical model. For consistency with the unperturbed Keplerian frame and in order to work with minimum dynamical masses, we assume an edge-on and coplanar configuration for the HD 202696 system (i.e., $i_{b,c} = 90^\circ$ and $\Delta\Omega = 0^\circ$). We find that the models are practically equivalent, suggesting a pair of planets with equal masses of the order of $\sim 2.0 M_{\text{Jup}}$ and a period ratio of $P_{\text{rat}} \approx 1.83$ near the 11:6 MMR (for details, see Table 3).

Both the Keplerian and dynamical fits reveal a moderate best-fit value of e_c for the eccentricity of the outer planet but with a large uncertainty toward nearly circular orbits. This indicates that e_c is likely poorly constrained, and perhaps this moderate eccentricity value is a result of overfitting. Indeed, a two-planet Keplerian model with circular orbits (i.e., $e_{b,c}, \omega_{b,c} = 0$) has $-\ln \mathcal{L} = 150.286$, meaning that the difference between the circular and noncircular Keplerian models is only $\Delta \ln \mathcal{L} \approx 1.5$, which is insignificant.¹¹ Thus, we conclude that neither the Keplerian nor the dynamical model applied to the current RV data can place tight constraints on the orbital eccentricities.

The inclusion of the planetary inclinations $i_{b,c}$ and $\Delta\Omega$ (i.e., Δi) in the dynamical modeling was also not justified. We find that all dynamical fits with coplanar inclinations in the range of $5^\circ < i_{b,c} < 90^\circ$ are practically indistinguishable from the coplanar and edge-on configuration ($i_{b,c} = 90^\circ$ and $\Delta\Omega = 0^\circ$). Fits with $i_{b,c} < 5^\circ$ are of poorer quality due to the increased dynamical masses of the companions and the strong gravitational interactions, which are not consistent with the data anymore. Therefore, any further attempt to constrain the planetary inclinations as coplanar or mutually inclined leads to inconclusive results.

Overall, our orbital parameter estimates show that taking the planetary gravitational interactions into account in the fitting does not yield a significant improvement over the Keplerian model. Yet we decide to rely on the dynamical modeling, since this scheme provides physical constraints on the derived orbital parameters and naturally penalizes highly unstable (unrealistic) orbital solutions.

4. Dynamical Characterization and Stability

4.1. Numerical Setup

The long-term stability and dynamical properties of the HD 202696 system are tested using the SyMBA N -body symplectic integrator (Duncan et al. 1998), which was modified to work in Jacobi coordinates (e.g., Lee & Peale 2003). We integrate each MCMC sample for a maximum of 1 Myr with a time step of 4 days. In case of planet–planet close encounters, however, SyMBA automatically reduces the time step to ensure an accurate simulation with high orbital resolution. SyMBA also checks for planet–planet or planet–star collisions or planetary ejections and interrupts the integration if they occur.

¹¹ Assuming that $2\Delta \ln \mathcal{L}$ follows a χ^2 distribution for nested models with $k = 4$ degrees of freedom (e.g., see Baluev 2009). Alternatively, the relative probability $R = e^{\Delta \ln \mathcal{L}}$ between two competing models constructed from the same parameters (relevant for the MCMC test) requires $\Delta \ln \mathcal{L} > 5$ to claim significance (see Anglada-Escudé et al. 2016).

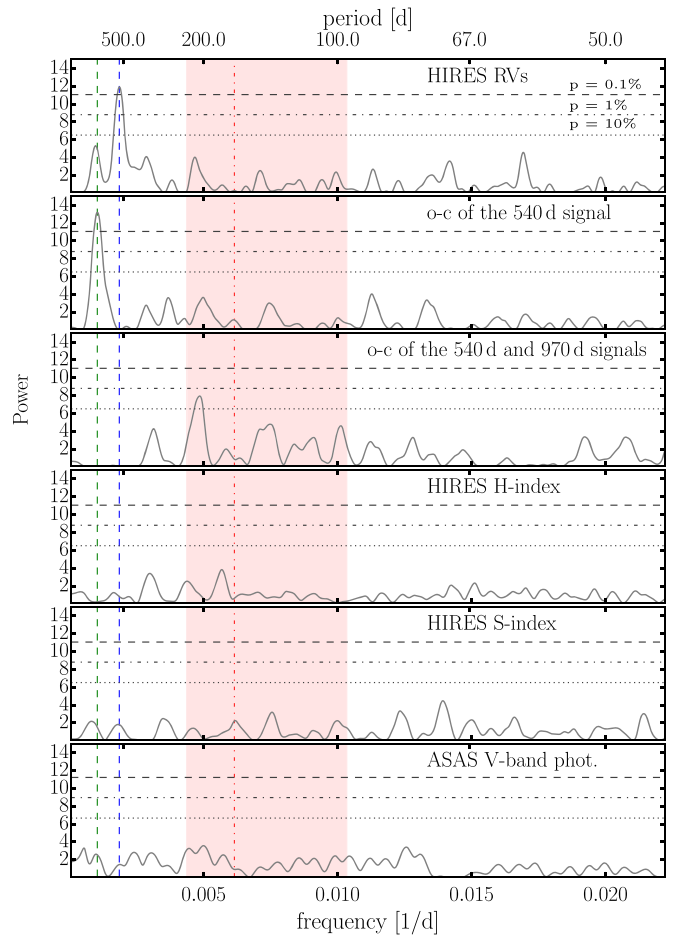


Figure 5. The GLS periodograms of the available HIRES RV time series reveal two significant signals around ~ 540 and ~ 970 days, marked with blue and green dashed lines, respectively. The possible stellar rotation frequencies are within the red shaded area, the red line denoting the most likely stellar rotation frequency (see Section 2). No evident periodicity with an FAP $< 0.1\%$ is detected after the prewhitening (i.e., consecutive subtraction of each signal from the data.) These two signals do not have counterparts in the S- and H-index activity indicators of the HIRES data, nor do they fall into the range of possible stellar rotational frequencies. The mean ASAS V-band photometry time series of HD 202696 is also clean of significant periodicities at these periods.

A planet is considered lost and the system unstable if, at any time: (i) the mutual planet–planet separation is below the sum of their physical radii (assuming Jupiter mean density), i.e., the planets undergo collision; (ii) the star–planet separation exceeds two times the initial semimajor axis of the outermost planet ($r_{\text{max}} > 2 \times a_{c \text{ in.}}$), which we define as planetary ejection; or (iii) the star–planet separation is below the physical stellar radius ($R \approx 0.03$ au), which we consider a collision with the star. All of these events are associated with large planetary eccentricities leading to crossing orbits, close planetary encounters, rapid exchange of energy and angular momentum, and eventually instability. Therefore, these somewhat arbitrary stability criteria are efficient to detect unstable configurations and save CPU time.

4.2. Stable Orbital Space

Figure 6 shows the posterior MCMC distribution of the fitted parameters with a dynamical modeling scheme whose orbital configuration is edge-on, coplanar, and stable for at least

Table 2
 HIRES Doppler Measurements for HD 202696 from Butler et al. (2017) and RV Residuals of the Best-fit Models from Table 3

Epoch (BJD)	RV (m s ⁻¹)	σ_{RV} (m s ⁻¹)	S Index	H Index	$o-c_{Kep.}$ (m s ⁻¹)	$o-c_{N-body}$ (m s ⁻¹)
2,454,287.927	2.88	1.96	0.1091	0.0312	-2.94	-3.57
2,454,399.822	-63.90	1.25	0.1072	0.0307	-2.53	-4.50
2,454,634.038	-20.49	1.14	0.0899	0.0312	-5.05	-5.41
2,454,674.900	2.57	1.39	0.1066	0.0308	-0.79	-0.85
2,454,718.006	10.64	1.49	0.0868	0.0308	-4.21	-4.00
2,454,777.857	11.66	1.19	0.1132	0.0309	-4.38	-3.84
2,454,778.819	13.33	1.39	0.1065	0.0308	-2.61	-2.07
2,454,805.740	10.92	1.40	0.1138	0.0308	-1.13	-0.41
2,454,955.107	-5.77	1.32	0.1055	0.0308	16.03	16.72
2,454,964.128	-15.69	1.23	0.1075	0.0310	7.25	7.84
2,454,984.066	-23.92	1.38	0.1065	0.0311	0.58	0.93
2,454,985.007	-26.07	1.40	0.1114	0.0309	-1.53	-1.20
2,455,014.963	-39.57	1.31	0.1072	0.0308	-15.66	-15.70
2,455,015.957	-41.36	1.31	0.1061	0.0310	-17.54	-17.59
2,455,019.021	-25.42	1.30	0.1143	0.0309	-1.89	-1.97
2,455,043.881	-18.51	1.40	0.1074	0.0307	1.18	0.87
2,455,076.033	-9.97	1.37	0.1129	0.0306	1.10	0.74
2,455,084.036	0.00	1.61	0.1251	0.0306	8.42	8.08
2,455,106.909	5.94	1.47	0.1086	0.0307	6.10	5.92
2,455,133.918	17.65	1.40	0.0936	0.0305	7.88	7.96
2,455,169.772	21.46	1.40	0.1145	0.0307	1.14	1.44
2,455,170.691	17.93	1.43	0.1069	0.0308	-2.59	-2.29
2,455,187.695	20.55	1.39	0.1011	0.0308	-2.85	-2.57
2,455,198.700	21.99	1.42	0.1075	0.0309	-2.35	-2.15
2,455,290.146	2.47	1.33	0.1010	0.0309	0.17	-1.29
2,455,373.126	-33.29	1.23	0.1137	0.0309	7.89	7.22
2,455,396.059	-52.38	1.36	0.1097	0.0309	-1.22	-1.26
2,455,436.743	-69.28	1.27	0.0975	0.0307	-5.03	-4.34
2,455,455.739	-73.42	1.34	0.1085	0.0307	-5.25	-4.49
2,455,521.793	-53.00	1.37	0.1062	0.0308	16.87	16.67
2,455,698.124	-10.58	1.35	0.1006	0.0309	-16.91	-17.80
2,455,770.042	53.71	1.56	0.1099	0.0309	28.09	27.74
2,455,787.946	20.04	9.66	0.0659	0.0285	-6.39	-6.71
2,455,841.869	26.89	1.26	0.0882	0.0308	5.86	5.65
2,455,880.836	8.95	1.23	0.1292	0.0312	-3.05	-3.06
2,455,903.717	-1.19	1.25	0.1071	0.0309	-6.85	-6.68
2,455,931.693	2.89	1.29	0.0945	0.0307	5.29	5.69
2,456,098.123	-28.24	1.31	0.1084	0.0309	-8.23	-7.59
2,456,154.011	-2.81	1.46	0.1084	0.0308	4.67	5.64
2,456,194.986	3.05	1.31	0.1098	0.0307	2.08	3.36
2,456,522.092	-57.44	1.43	0.1149	0.0309	1.73	0.45
2,456,894.081	19.32	1.23	0.1113	0.0309	-5.09	-5.03

1 Myr. The histogram panels in Figure 6 provide a comparison between the probability density distribution of the overall MCMC samples (black) and the stable samples (red) for each fitted parameter. The two-dimensional parameter distribution panels represent all possible parameter correlations with respect to the best dynamical fit from Table 2, whose position is marked with blue lines. The black 2D contours are constructed from the overall MCMC samples (gray) and indicate the 68.3%, 95.5%, and 99.7% confidence levels (i.e., 1σ , 2σ , and 3σ). For clarity, in Figure 6, the stable samples are overplotted in red.

We find that $\sim 46\%$ of the MCMC samples are stable. The histograms in Figure 6 clearly show that the distributions of all MCMC samples and their stable counterparts are in mutual agreement, peaking near the position of the best dynamical fit. The main exception is the distribution of e_c , which is bimodal with a stronger peak suggesting nearly circular orbits and a

smaller peak at somewhat moderate eccentricities from where the best dynamical fit originates. Here P_b and ω_b also show bimodal distributions, which are related to the bimodal distribution of e_c . As we discussed in Section 3.2, however, the best-fit eccentricities are statistically insignificant, and a simpler two-planet model with circular orbits is equally good in terms of $-\ln \mathcal{L}$. This indicates that the best-fit solution is likely a global $-\ln \mathcal{L}$ minimum, which lies in a smaller and isolated orbital parameter space with moderate e_c . This minimum and its surroundings, however, are highly unstable and therefore unlikely to represent the HD 202696 system configuration. Thus, running an MCMC test reveals a larger, stable, and statistically confident orbital parameter space toward $e_{b,c} \rightarrow 0$, where the stable fraction of the sample distribution is $\sim 75\%$. From the long-term dynamical analysis of the posterior MCMC samples, we can place a boundary at planetary eccentricities $e_{b,c} \leq 0.1$, while larger eccentricities are very unlikely. The

overall posterior distribution of $\omega_{b,c}$ and $M_{b,c}$ are consistent with the best-fit estimate, but the stability test cannot constrain these parameters. Because of the low eccentricities of the stable solutions, these parameters are ambiguous and can be found anywhere between 0° and 360° . However, the orbital mean longitudes $\lambda_{b,c} = \omega_{b,c} + M_{b,c}$ are rather well constrained to $\sim \pm 50^\circ$ (see Table 3).

Given the stability constraints from our MCMC test, the most realistic configuration of the HD 202696 system is represented by the parameter distribution of the stable fits. In Table 4, we present our final orbital estimates of the two-planet system assuming coplanar and edge-on ($i_{b,c} = 90^\circ$, $\Delta\Omega = 0^\circ$) configurations. These parameters are adopted from the maximum value of the stable parameter probability density function, while the uncertainties are the 0.16 and 0.84 quantiles of the distribution. Our new orbital estimate is consistent with circular orbits $e_b = 0.011^{+0.078}_{-0.011}$ and $e_c = 0.029^{+0.065}_{-0.012}$ but otherwise consistent with the best two-planet dynamical fit shown in Table 3.

Integrating this configuration for 100 Myr reveals a stable planetary system with a mean period ratio $\overline{P_{\text{rat}}} \approx 1.83$ and orbital eccentricities oscillating in opposite phase in the range from 0 to 0.05 for e_b and 0 to 0.04 for e_c . This configuration librates mostly in an anti-aligned geometry with a secular apsidal angle $\Delta\omega = \omega_b - \omega_c \sim 180^\circ$ exhibiting a large libration amplitude of $\pm 80^\circ$.

The long-term stability of the orbital estimate shown in Table 4 boosts the confidence that the most likely orbital configuration of the HD 202696 system has been identified.

4.3. Stability Constraints on the Planetary Masses

While the dynamical modeling of the HIRES Doppler measurements of HD 202696 was unable to qualitatively constrain the masses of HD 202696 b and c, we also use the long-term stability of fits with forced inclination as an efficient way to limit the range of the possible planetary masses further. Figure 7 shows the results from this test. We inspect the range of inclinations from $i = 90^\circ$ to 5° . To ensure enhanced stability, we adopt the planetary eccentricity estimates from Table 4, which, for each adopted i , remained fixed in the fit. The small $\Delta \ln \mathcal{L}$ of the dynamical models in the range of $i = 90^\circ - 15^\circ$ shows that these models are statistically equivalent, but the fit quality rapidly deteriorates for $i < 15^\circ$ (not shown in Figure 7). This is likely due to the significantly increased planetary masses, which may alter the system stability even at lower eccentricities.

Inclination $i = 20^\circ$ seems to be a stability boundary of the coplanar case, leaving the companion masses in the planetary regime with a maximum of about three times the minimum planetary masses of the coplanar edge-on case. However, since orbital inclinations near $i = 90^\circ$ are statistically more likely, we limit our dynamical analysis of the HD 202696 system to the coplanar and edge-on configuration.

4.4. Dynamical Properties of the Stable MCMC Samples

Overall dynamical analysis of the stable samples reveals that the mean period ratio over 1 Myr of integrations is $\overline{P_{\text{rat}}} = 1.83^{+0.04}_{-0.05}$, which is consistent with the period ratio from which the system is initially integrated, $P_{\text{rat.in}} = 1.82^{+0.03}_{-0.03}$. This implies that the stable MCMC orbital configurations remain regular and well separated at any given time of the stability test.

From these stable samples, $\sim 29\%$ are found with an aligned apsidal libration ($\Delta\omega \sim 0^\circ$), $\sim 34\%$ in an anti-aligned apsidal libration ($\Delta\omega \sim 180^\circ$; similar to the orbital evolution of the long-term stable configuration presented in Table 4), and $\sim 37\%$ in apsidal circulation ($\Delta\omega$ in the range $0^\circ - 360^\circ$). In fact, the latter case usually involves e_b decreasing from near its maximum value to near zero and e_c increasing from near zero to near its maximum value at $\Delta\omega \approx 90^\circ$, and vice versa at $\Delta\omega \approx 270^\circ$, with episodes of rapid circulation when e_b or e_c is nearly zero (see right panel of Figure 9). This type of evolution is consistent with a phase space dominated by large libration islands about $\Delta\omega = 0^\circ$ and 180° and having only a narrow region of circulation (see, e.g., Lee & Peale 2003).

Figure 8 shows the distribution of the mean period ratio $\overline{P_{\text{rat}}}$ and the libration amplitudes of $\Delta\omega$ for the stable dynamical samples with aligned apsidal libration $\Delta\omega \sim 0^\circ$ (left panel) and anti-aligned apsidal libration $\Delta\omega \sim 180^\circ$ (right panel). From Figure 8, it is clear that both alignment and anti-alignment have similar libration amplitudes of $\Delta\omega$ peaking around 70° and with a sharp border at 90° , beyond which the system is involved in apsidal circulation. An interesting pileup in the posterior distribution of $\overline{P_{\text{rat}}}$ can be seen around 1.80, 1.83, and 1.86, which correspond to the 9:5, 11:6, and 13:7 MMRs. We inspected these possible high-order MMRs for librating resonance angles,¹² but we did not detect any. Despite the apsidal libration of the $\Delta\omega$ in $\sim 60\%$ of the configurations, which is suggestive of resonant behavior, the system seems to be out of any MMR. In the $\Delta\omega \sim 180^\circ$ case, a small number of system configurations are consistent with a 2:1 period ratio, but these samples have statistically poorer $-\ln \mathcal{L}$ and are thus unlikely to represent the HD 202696 system.

Given the large fraction of nonresonant stable configurations, we concluded that the system HD 202696 is most likely dominated by secular interactions at low eccentricities. Figure 9 shows the orbital evolution of three confident stable configurations that have a mean period ratio of $\overline{P_{\text{rat}}} \sim 1.83$ exhibiting $\Delta\omega \sim 0^\circ$, $\Delta\omega \sim 180^\circ$, and $\Delta\omega$ circulating, respectively. The various stable configurations show libration amplitudes in their eccentricities between 0 and 0.15 but with mean values consistent with the posterior eccentricity distribution. The secular timescales of these oscillations strongly depend on the initial orbital geometries and planetary masses, ranging mostly between ~ 200 and ~ 1000 yr.

5. Discussion

5.1. Tight Jovian Pairs around Evolved Stars

The HD 202696 system is another example of a growing number of multiplanetary systems around evolved intermediate-mass stars with semimajor axes close to the critical stability boundary. Including HD 202696, there are now seven tightly packed planetary systems with period ratios smaller than or about 2:1.

Earlier examples are the 24 Sex and HD 200964 systems (Johnson et al. 2011). A $1.5 M_\odot$ subgiant, 24 Sex is orbited by two Jovian planets with minimum dynamical masses of $m_b \sim 2$ and $m_c \sim 0.9 M_{\text{Jup}}$ and periods of $P_b \approx 450$ and $P_c \approx 883$ days. The best-fit period ratio for the 24 Sex system is

¹² For the $m:n$ MMR, the resonance angles are defined as $\theta_{k=1,m-n} = n\lambda_b + (n-k)\varpi_b - m\lambda_c - (1-k)\varpi_c$, where ϖ and λ are the planetary longitude of periastron and the mean longitude, respectively. At least one resonance angle θ_k must librate to claim an MMR configuration.

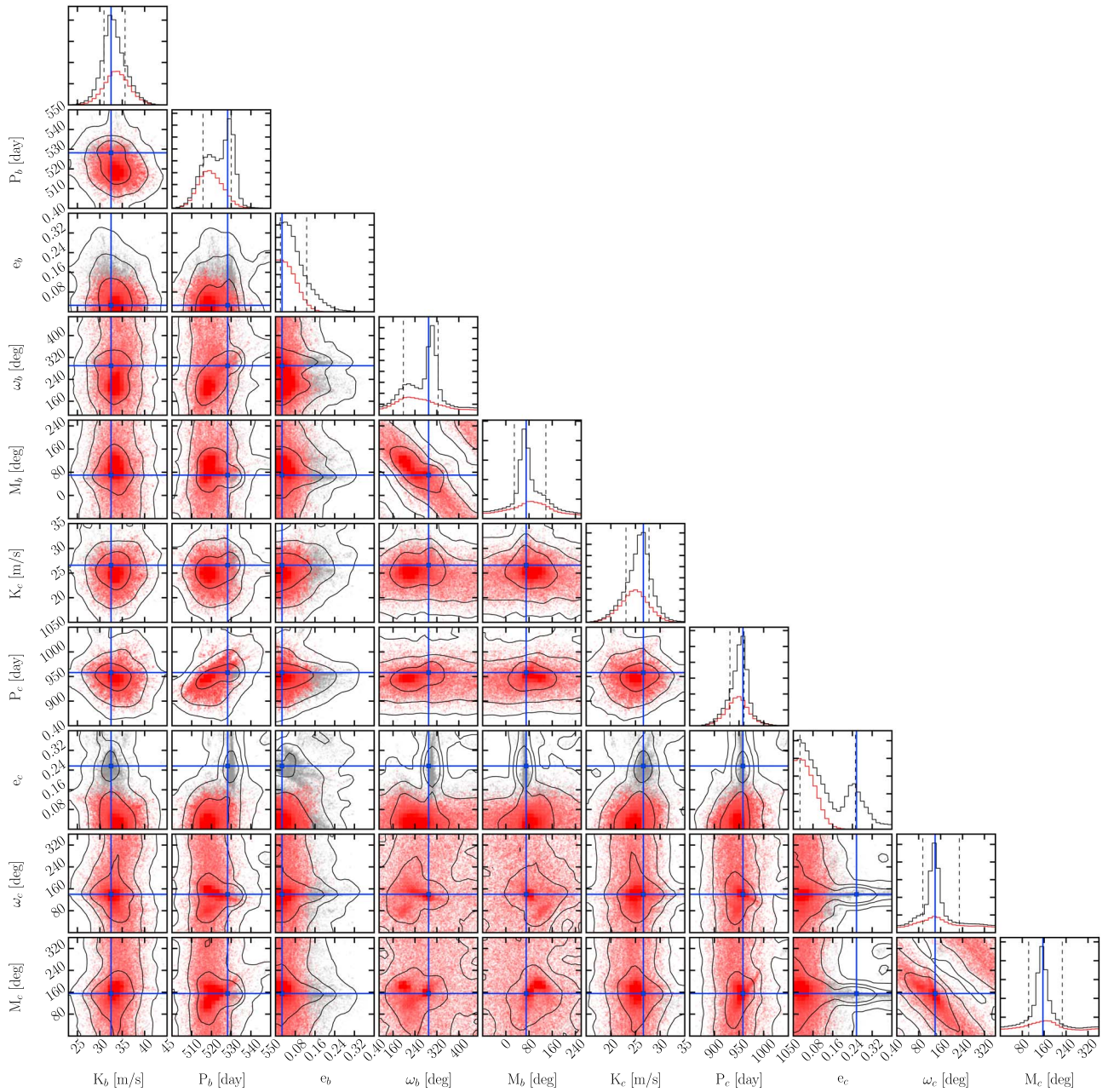


Figure 6. The MCMC distribution of orbital parameters consistent with the HIRES RV data of HD 202696, assuming an edge-on coplanar two-planet system fitted with a self-consistent dynamical model. The position of the best dynamical fit from Table 3 is marked with blue lines. The black contours on the 2D panels represent the 1σ , 2σ , and 3σ confidence levels of the overall MCMC samples, while on the 1D histograms, the dashed lines mark the 16th and 84th percentiles of the overall MCMC samples. The samples that are stable for at least 1 Myr are red and represent $\sim 46\%$ of all samples. The stable samples are mostly within the 1σ confidence region from the best fit. See the text for details.

slightly below 2:1, but the planets are almost certainly involved in a 2:1 MMR (Johnson et al. 2011; Wittenmyer et al. 2012). The HD 200964 system is similar to 24 Sex in terms of stellar mass and minimum planetary masses, but it has a much more compact orbital configuration, with periods of $P_b \approx 610$ and $P_c \approx 830$ days. The HD 200964 system is only stable if the orbits are in a 4:3 MMR (Wittenmyer et al. 2012; Tadeu dos Santos et al. 2015).

The $1.5 M_\odot$ subgiant star HD 5319 is another 4:3 MMR candidate host (Robinson et al. 2007; Giguere et al. 2015). With minimum planetary masses of $m_b \sin i \sim 1.8$ and $m_c \sin i \sim 1.2 M_{\text{Jup}}$ and periods of $P_b \approx 640$ and $P_c \approx 890$ days, this system is dynamically very challenging. Giguere et al. (2015)

showed that, although most of the possible configurations of HD 5319 are unstable, stable solutions at the exact 4:3 MMR do exist. Therefore, the 4:3 MMR seems like the most reasonable explanation of the coherent Doppler signal of HD 5319.

A $1.7 M_\odot$ slightly evolved star, HD 33844 was reported by Wittenmyer et al. (2016) to host two Jovian-mass planets with minimum dynamical masses $m_b \sim 1.9$ and $m_c \sim 1.7 M_{\text{Jup}}$ and periods of $P_b \approx 550$ and $P_c \approx 920$ days. These authors concluded that the planetary pair is most likely trapped in the 5:3 MMR, but stable solutions consistent with 8:5 and 12:7 MMR were also found within the 1σ uncertainty in the semimajor axes.

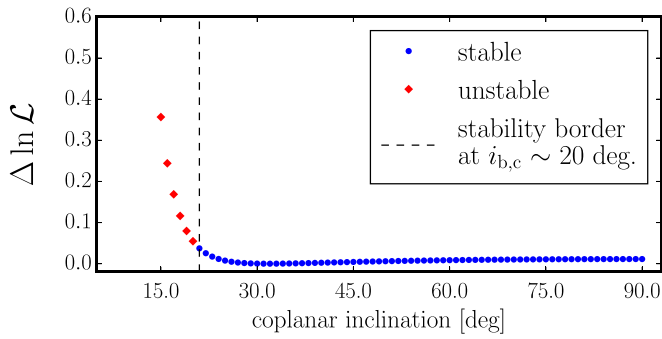


Figure 7. Coplanar dynamical fits with nearly circular orbits as a function of inclination. The stability boundary is at $i = 20^\circ$, which sets a planetary mass limit of approximately three times the minimum planetary mass of the edge-on coplanar case (e.g., see Table 4).

A $1.8 M_\odot$ giant, HD 47366 has two nearly equal-mass planetary companions (Sato et al. 2016). With $m_b \sin i \sim 1.8$ and $m_c \sin i \sim 1.9 M_{\text{Jup}}$ and periods of $P_b \approx 363$ and $P_c \approx 685$ days, the system is dynamically challenging. Within the uncertainties of the orbital parameters given, the initial period ratio is close to 15:8, where the system could be stable if the planets are on circular orbits. Sato et al. (2016) also proposed that HD 47366 could be locked in a retrograde 2:1 MMR. Tightly packed retrograde configurations are, however, difficult to reconcile with current planet formation scenarios. Marshall et al. (2019) showed that alternatives to these configurations for HD 47366 exist, including stable prograde solutions in the 2:1 MMR.

The η Ceti system is composed of a giant star orbited by a planet pair with minimum dynamical masses of $m_b \sim 2$ and $m_c \sim 3 M_{\text{Jup}}$ and nominal best-fit periods of $P_b \approx 400$ and $P_c \approx 750$ days. Trifonov et al. (2014) found two possible stability regimes for η Ceti: either it is a strongly interacting two-planet system locked in an anti-aligned 2:1 MMR or, with lower probability, it could be a low-eccentricity two-planet system dominated by secular interactions close to a high-order MMR like 9:5, 11:6, 13:7, or 15:8, resembling to some extent the HD 202696 system.

Figure 10 shows all known RV multiple-planet systems around intermediate-mass stars with masses larger than $1.3 M_\odot$.¹³ The stellar host mass is shown as a function of the logarithm of the system’s period ratio. A total of 21 planetary¹⁴ systems are shown in Figure 10. The seven planetary systems found between the 2:1 and 4:3 first-order MMRs (and briefly described above) represent 33% of all known massive multiple-planet systems around intermediate-mass stars. This fraction is rather large given the broad range of the observed planetary period ratios. The planet pair occurrence rate at low period ratios, of course, could be a result of a selection effect, since these systems are likely to be discovered first by precise Doppler surveys. However, a more intriguing possibility is that the increasing number of these tight planetary pairs indicates the existence of a massive multiple-planet system population, some of which have successfully broken the 2:1 MMR during the planet migration phase.

¹³ Taken from <http://exoplanet.eu>, regardless of their spectral type and evolutionary stage.

¹⁴ As can be seen from Figure 10, one of the systems is in fact a brown dwarf pair. This is the ν Oph system locked in a 6:1 MMR (Quirrenbach et al. 2011; Sato et al. 2012; Quirrenbach et al. 2019).

Table 3
Best Keplerian and Dynamical Fits for the HD 202696 System

Two-planet Keplerian Model		
Parameter	HD 202696 b	HD 202696 c
Semi-amplitude K [m s ⁻¹]	31.7 ^{+4.8} _{-2.1}	28.1 ^{+1.1} _{-5.3}
Period P [days]	521.0 ^{+6.2} _{-7.3}	956.1 ^{+22.4} _{-29.9}
Eccentricity e	0.056 ^{+0.066} _{-0.040}	0.261 ^{+0.060} _{-0.202}
Arg. of periastron ω [deg]	259.2 ^{+106.0} _{-89.2}	129.1 ^{+142.7} _{-33.6}
Mean anomaly M_0 [deg]	69.7 ^{+85.8} _{-115.8}	152.0 ^{+112.8} _{-74.3}
Mean longitude λ [deg]	328.8 ^{+50.4} _{-44.9}	281.1 ^{+50.5} _{-58.9}
Semimajor axis a [au]	1.573 ^{+0.012} _{-0.015}	2.357 ^{+0.037} _{-0.049}
Minimum mass $m \sin i$ [M_{Jup}]	1.930 ^{+0.285} _{-0.132}	2.028 ^{+0.073} _{-0.354}
RV offset [m s ⁻¹]		-15.32 ^{+2.59} _{-1.15}
RV jitter [m s ⁻¹]		8.20 ^{+3.07} _{-0.46}
$-\ln \mathcal{L}$		148.799
Two-planet Dynamical Model		
Parameter	HD 202696 b	HD 202696c
Semi-amplitude K [m s ⁻¹]	32.5 ^{+3.1} _{-1.6}	26.6 ^{+1.1} _{-3.5}
Period P [days]	528.2 ^{+1.8} _{-12.5}	958.0 ^{+2.2} _{-26.4}
Eccentricity e	0.026 ^{+0.100} _{-0.006}	0.265 ^{+0.005} _{-0.229}
Arg. of periastron ω [deg]	289.7 ^{+35.1} _{-91.8}	140.0 ^{+88.7} _{-44.9}
Mean anomaly M_0 [deg]	70.2 ^{+67.9} _{-40.8}	155.5 ^{+70.41} _{-52.2}
Mean longitude λ [deg]	359.9 ^{+8.2} _{-63.0}	259.5 ^{+1.0} _{-68.5}
Semimajor axis a [au]	1.587 ^{+0.004} _{-0.025}	2.360 ^{+0.003} _{-0.040}
Min. dyn. mass m [M_{Jup}]	1.991 ^{+0.174} _{-0.011}	1.917 ^{+0.116} _{-0.212}
Inclination i [deg]	90.0 (fixed)	90.0 (fixed)
Node $\Delta\Omega$ [deg]		0.0 (fixed)
RV offset [m s ⁻¹]		-15.12 ^{+1.95} _{-1.44}
RV jitter [m s ⁻¹]		8.31 ^{+3.08} _{-0.47}
$-\ln \mathcal{L}$		148.973

Note. The parameters are valid for BJD = 2,450,000 and are derived using our stellar mass estimate of $M = 1.91 M_\odot$. The uncertainties of $a_{b,c}$, $m_{b,c} \sin i$ (Keplerian model), and $m_{b,c}$ (dynamical model) do not take into account the small uncertainty of the stellar mass.

It should be noted that a strongly interacting 2:1 MMR system could, in principle, exhibit prominent oscillations of its semimajor axis (and period ratio). The secular oscillation timescales are usually longer than the temporal baseline of the Doppler measurements and therefore normally only marginally detected in the best-fit modeling. An example is the η Ceti system, where best-fit dynamical modeling of the osculating orbits suggests $\overline{P_{\text{rat.}}} \sim 1.86$, but the stable solutions of the system have $\overline{P_{\text{rat.}}} = 2:1$, with an MMR libration amplitude of $\Delta \overline{P_{\text{rat.}}} \sim 0.2$ and timescales of ~ 500 yr (Trifonov et al. 2014). In this context, the 24 Sex, HD 47366, and even HD 202696 systems could in fact be true 2:1 MMR systems with oscillating period ratios, observed slightly below the 2:1 period ratio at the present epoch. More precise Doppler data for these systems taken in the future, with an extended temporal baseline, could reveal the true orbital configurations of these systems; we encourage such extended RV campaigns. Still, the HD 33844 system is likely stable at or near the 5:3 MMR, while the HD 5319 and HD 200964 planetary systems can only be stable if they are involved in the 4:3 MMR. The latter systems are dynamically not consistent with the 2:1 MMR and thus indicate that planet pairs could break the 2:1 MMR and settle at other stable orbits in lower-order MMRs.

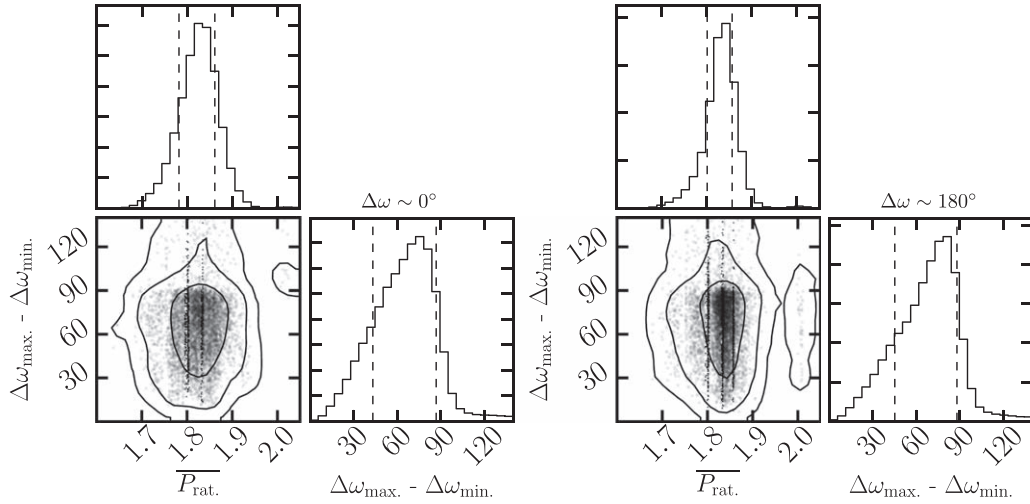


Figure 8. Distribution of the mean period ratio $\overline{P}_{\text{rat}}$ and the amplitude of the apsidal argument $\Delta\omega$ for all dynamical fits that are stable up to 1 Myr (see Figure 6) and consistent with libration of $\Delta\omega$. The left panel shows those stable samples whose dynamical properties are consistent with aligned apsidal libration ($\Delta\omega \sim 0^\circ$), while the right panel shows the samples with anti-aligned apsidal libration ($\Delta\omega \sim 180^\circ$). Both geometries are consistent with $\overline{P}_{\text{rat}} \sim 1.83$ (near 11:6 MMR) and have similar $\Delta\omega$ libration amplitudes. Sample concentrations near the 9:5 and 13:7 MMRs (slightly enhanced) are also within the 1σ confidence levels of the stable posterior distribution. A small and insignificant fraction of the samples are found in the 2:1 MMR.

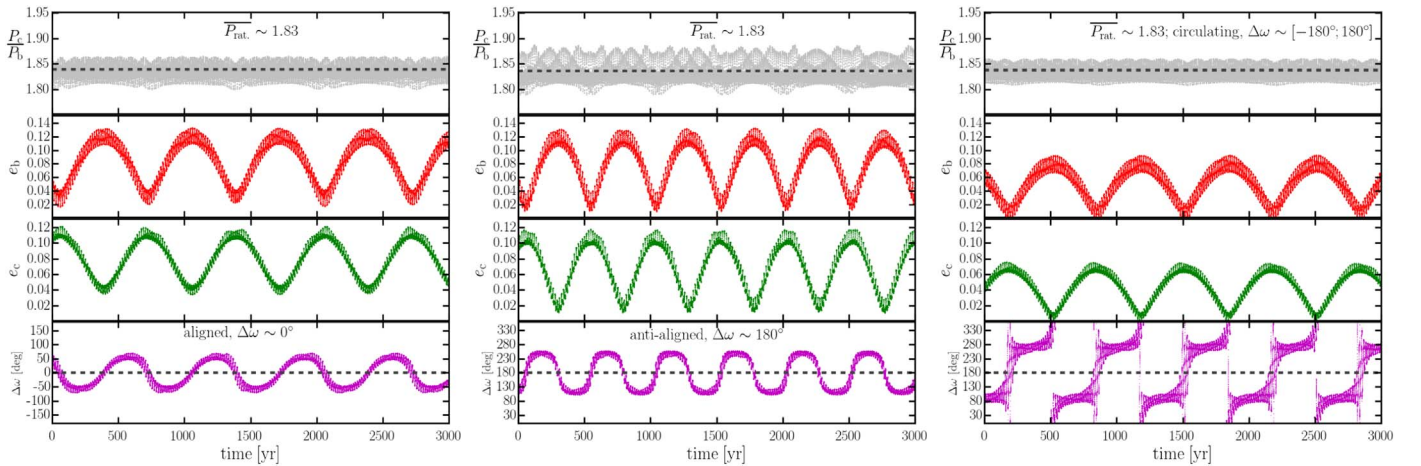


Figure 9. Reconstruction of three possible outcomes of the orbital evolution of the HD 202696 system with $\overline{P}_{\text{rat}} \sim 1.83$, randomly chosen from the stable posterior distribution. Left panel: orbital evolution with $\Delta\omega$ librating around 0° . Middle panel: a case where $\Delta\omega$ librates around 180° . Right panel: a case where $\Delta\omega$ circulates between 0° and 360° . Note the large amplitude of P_{rat} in all three cases.

5.2. Planetary Migration below the 2:1 MMR

The HD 202696 system, like the majority of the known Jovian-mass planetary systems, is currently located within the so-called “ice line,” where it is unlikely to form gas giants. This can be easily seen from Figure 11, which shows the planetary systems from Figure 10 versus their planetary semimajor axes. The dashed blue line denotes the approximate ice-line radius, beyond which it is commonly accepted that planetary embryos are able to accumulate icy material and grow massive enough to start gas accretion from the protoplanetary disk to eventually become Jovian-mass planets. While accreting disk material, massive planets undergo inward migration toward the stellar host before the disk dissipates, and planets end up at their observed semimajor axes. We note that the ice line plotted in Figure 11 is calculated for the protoplanetary phase assuming only stellar irradiation, where the disk temperature would be $T_{\text{irr}} = 150$ K (Ida et al. 2016), but adopting a stellar mass–luminosity relation of the form $L = M^{3.5}$, which is reasonable

for main-sequence stars. We are aware that this is a crude approximation, but it is sufficient to demonstrate the generally “warm orbits” of the discovered Jovian-mass planets orbiting intermediate stars.

Figure 11, in connection with current planet formation theories, suggests that the massive planet pairs have formed further out than observed today and have migrated inward together. If the migration is convergent, there is a high probability of planets being trapped in an orbital resonance, with a final stop at the strong 2:1 MMR (e.g., Lee & Peale 2002; Beaugé et al. 2003). Perhaps due to not yet well understood dynamical processes between the disk and the planets, pairs of planets may have broken the 2:1 MMR and migrated further in.

André & Papaloizou (2016) studied systems similar to 24 Sex and η Ceti and were able to reproduce the 2:1 MMR in these systems. However, in their simulations, there were also cases in which the planets passed through the 2:1 MMR,

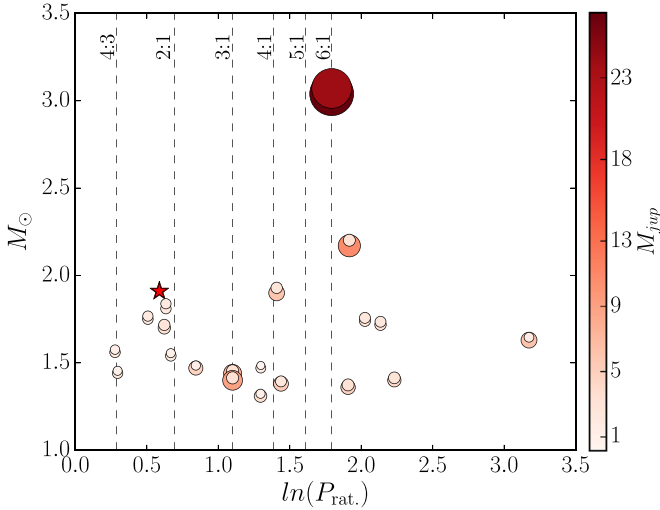


Figure 10. Period ratio of known multiplanetary systems discovered via the Doppler method and orbiting stars with estimated masses larger than $1.3 M_{\odot}$. Each planetary companion is plotted at the published best-fit period ratio for the system, with a symbol that is color-coded and scaled in size with its reported mass. Six dynamically challenging systems are known to orbit at or below the 2:1 MMR. A new member of this sample with a period ratio of 11:6, HD 202696 is indicated in the plots with a red star symbol. See text for details.

Table 4

Mode of the Dynamically Stable MCMC Distribution for the HD 202696 System (Peak of the Red Histograms from Figure 6)

Adopted Two-planet Coplanar Edge-on Configuration Based on Stability		
Parameter	HD 202696 b	HD 202696c
Semi-amplitude K [m s^{-1}]	$34.1^{+2.3}_{-2.9}$	$25.3^{+2.1}_{-3.3}$
Period P [days]	$517.8^{+8.9}_{-3.9}$	$946.6^{+20.7}_{-20.9}$
Eccentricity e	$0.011^{+0.078}_{-0.011}$	$0.028^{+0.065}_{-0.012}$
Arg. of periastron ω [deg]	$201.6^{+97.8}_{-98.5}$	$136.8^{+143.0}_{-62.7}$
Mean anomaly M_0 [deg]	$79.2^{+198.6}_{-28.1}$	$180.0^{+98.9}_{-108.9}$
Mean longitude λ [deg]	$298.8^{+70.0}_{-14.6}$	$262.8^{+37.8}_{-53.3}$
Semimajor axis a [au]	$1.566^{+0.016}_{-0.007}$	$2.342^{+0.034}_{-0.035}$
Dyn. mass m [M_{Jup}]	$1.996^{+0.220}_{-0.100}$	$1.864^{+0.177}_{-0.227}$
Inclination i [deg]	90.0 (fixed)	90.0 (fixed)
Node $\Delta\Omega$ [deg]	0.0 (fixed)	
RV offset [m s^{-1}]	$-14.42^{+1.70}_{-2.22}$	
RV jitter [m s^{-1}]	$9.36^{+2.93}_{-0.57}$	

Note. Same comments as in Table 3.

which made them undergo capture into the destabilizing 5:3 resonance. André & Papaloizou (2016) concluded that finding systems in the 5:3 MMR is unlikely.

In this context, the 4:3 MMR systems are also very challenging from the formation perspective. Rein et al. (2012) failed to reproduce the 4:3 MMR of the HD 200964 system using the standard formation scenarios, such as convergent migration, scattering, and in situ formation. On the other hand, Tadeu dos Santos et al. (2015) were able to closely reproduce the 4:3 resonant dynamics of HD 200964 by including interactions between type I and type II migration, planetary growth, and stellar evolution. As pointed out by Tadeu dos Santos et al. (2015), however, the 4:3 MMR capture of the HD 200964 system occurred only for a very narrow range of initial conditions.

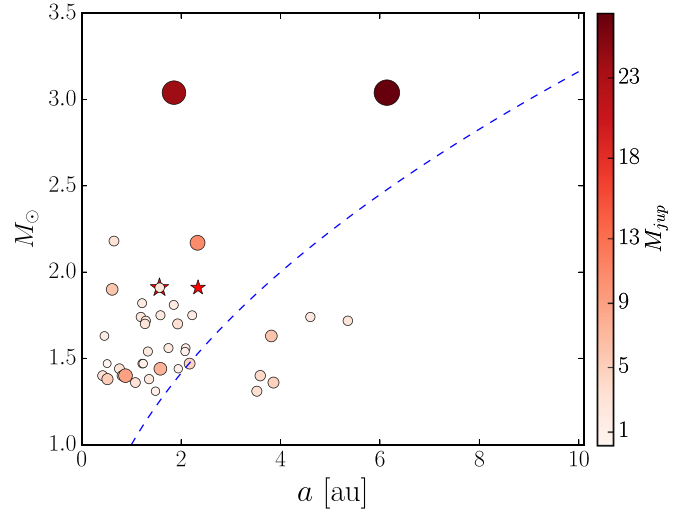


Figure 11. Same as Figure 10 but as a function of the planetary semimajor axis. The dashed blue curve shows the approximate position of the pre-main-sequence “ice line” for stellar masses between 1 and $3.5 M_{\odot}$. Most of the discovered Jovian-mass multiple-planet systems around intermediate-mass stars are within the ice line, suggesting that these pairs most likely migrated inward together during the disk phase. See text for details.

In general, massive planets that have reached the gap opening mass migrate via type II migration, which follows the viscous disk evolution (Lin & Papaloizou 1986). In this case, a two-planet pair would migrate on the same timescale, and it is very hard for the outer planet to catch up with the inner planet, let alone to break free from a resonance trapping via planet-disk interactions.

However, if the outer planet is less massive and does not open a full gap, it can undergo type III migration (Masset & Papaloizou 2003). This migration mode is even faster than type I migration and can easily allow outer planets to catch up with inner, more massive planets and be trapped in resonance (Masset & Snellgrove 2001).

This situation has been studied in the framework of the Grand-Tack scenario for Jupiter and Saturn (Walsh et al. 2011; Pierens et al. 2014). In particular, Pierens et al. (2014) found that the inward-migrating Saturn could, under certain disk conditions, have broken free from the 2:1 resonance and migrated closer to Jupiter, where trapping could have occurred, e.g., in the 3:2 resonance.

While the planets are still embedded in the gas disk, they will continue to accrete gas and grow. The outer planet can feed from a larger gas reservoir than the inner one because it has direct access to the disk’s gas supply with the full disk accretion rate. The inner planet can only accrete the gas that passed the outer planet, which is typically only up to 20% of the disk’s accretion rate (Lubow & D’Angelo 2006). Eventually, the outer planet can outgrow the inner planet if the disk lifetime is long enough. During their final growth, the dynamical interactions between the giant planets change, which could lead to small orbital disturbances breaking the final resonance.

A possible escape from the 2:1 MMR could also be a resonance overstability, as in the context of Goldreich & Schlichting (2014). In this case, convergent planetary migration with strongly damped eccentricities may only lead to a temporal capture at the 2:1 MMR. However, these scenarios require further investigation, which is beyond the scope of this paper.

6. Summary

The star HD 202696 is an early K0 giant ($M = 1.91_{-0.14}^{+0.09} M_{\odot}$, $\log g = 3.24 \pm 0.15 \text{ cm s}^{-2}$, $[\text{Fe}/\text{H}] = 0.02 \pm 0.04 \text{ dex}$) for which HIRES high-precision RV measurements were taken between 2007 and 2014. The RV data indicate the presence of at least two strong periodicities near 520 and 940 days, with no evidence of stellar activity near these periods. Therefore, the most plausible explanation of the observed RVs is stellar reflex motion induced by a pair of Jovian-mass planets, each with a minimum mass of $\sim 2 M_{\text{Jup}}$.

Dynamical modeling of the RV data is particularly important for the HD 202696 system, since planet–planet perturbations in this relatively compact system of massive planets cannot be neglected. For the orbital analysis, we therefore rely on a self-consistent dynamical scheme for the RV modeling, coupled with an MCMC sampling algorithm for parameter analysis. Each MCMC orbital configuration was further integrated with the SyMBA *N*-body integrator for a maximum of 1 Myr to analyze the long-term stability and dynamical properties of the system.

Our long-term stability results yield that approximately 46% of the edge-on coplanar ($i = 90^{\circ}$, $\Delta\Omega = 0^{\circ}$) MCMC samples survived 1 Myr. The stable parameter space of confident MCMC configurations suggests planets on nearly circular orbits with (minimum) dynamical masses of $m_b = 2.0_{-0.10}^{+0.22}$ and $m_c = 1.86_{-0.23}^{+0.18} M_{\text{Jup}}$. The planetary semimajor axes are $a_b = 1.57_{-0.01}^{+0.02}$ and $a_c = 2.34_{-0.04}^{+0.03}$ au, forming a period ratio of $\sim 11:6$, which is preserved during the numerical orbital evolution. Overall, we find that the HD 202696 system is most likely dominated by secular perturbations near the 11:6 mean-motion commensurability, with no direct evidence of resonance motions.

In this context, the HD 202696 system is not unique. It belongs to a population of massive multiplanet systems orbiting evolved intermediate-mass stars with orbital period ratios between the first-order MMRs of 2:1 and 4:3. These systems impose challenges for planet migration theories, since during the type II migration phase, they unavoidably must have passed through the strong 2:1 MMR, which requires special conditions for each case and thus in general has a low probability. Understanding the giant-planet migration into high-order MMR commensurability after passing the strong 2:1 MMR, as in the case of the HD 202696 system, requires more sophisticated disk–planet migration simulations, which are beyond the scope of this study.









The discovery of more multiplanet systems around G and K giants will be important to better understand planet formation and evolution around more massive and evolved stars.

This work was supported by the DFG Research Unit FOR 2544, *Blue Planets around Red Stars*, project No. RE 2694/4-1. S.R. further acknowledges the support of the DFG Priority Program SPP 1992, *Exploring the Diversity of Extrasolar Planets* (RE 2694/5-1). M.H.L. was supported in part by Hong Kong RGC grant HKU 17305015. B.B. thanks the European Research Council (ERC Starting grant 757448-PAMDORA) for their financial support. This research has made use of the SIMBAD database, operated at CDS, Strasbourg, France. This work has made use of data from the European Space Agency (ESA) mission *Gaia* (<https://www.cosmos.esa.int/gaia>), processed by the *Gaia* Data Processing and Analysis Consortium (DPAC; <https://www.cosmos.esa>

<https://www.cosmos.esa>). Funding for the DPAC has been provided by national institutions, in particular the institutions participating in the *Gaia* Multilateral Agreement. We also wish to extend our special thanks to those of Hawaiian ancestry on whose sacred mountain of Maunakea we are privileged to be guests. Without their generous hospitality, the Keck observations presented herein would not have been possible. We thank the anonymous referee for the excellent comments that helped to improve this paper.

Software: CERES pipeline (Brahm et al. 2017a), ZASPE (Brahm et al. 2017b), astroML (VanderPlas et al. 2012), Systemic Console (Meschiari et al. 2009), emcee (Foreman-Mackey et al. 2013).

ORCID iDs

Trifon Trifonov  <https://orcid.org/0000-0002-0236-775X>
 Stephan Stock  <https://orcid.org/0000-0002-1166-9338>
 Thomas Henning  <https://orcid.org/0000-0002-1493-300X>
 Sabine Reffert  <https://orcid.org/0000-0002-0460-8289>
 Martin Kürster  <https://orcid.org/0000-0002-1765-9907>
 Man Hoi Lee  <https://orcid.org/0000-0003-1930-5683>
 Bertram Bitsch  <https://orcid.org/0000-0002-8868-7649>
 R. Paul Butler  <https://orcid.org/0000-0003-1305-3761>
 Steven S. Vogt  <https://orcid.org/0000-0001-7177-7456>

References

- André, Q., & Papaloizou, J. C. B. 2016, *MNRAS*, 461, 4406
 Anglada-Escudé, G., Amado, P. J., Barnes, J., et al. 2016, *Nature*, 536, 437
 Arenou, F., & Luri, X. 1999, in ASP Conf. Ser. 167, Harmonizing Cosmic Distance Scales in a Post-HIPPARCOS Era, ed. D. Egret & A. Heck (San Francisco, CA: ASP), 13
 Bailer-Jones, C. A. L., Rybizki, J., Fouesneau, M., Mantelet, G., & Andrae, R. 2018, *AJ*, 156, 58
 Baluev, R. V. 2009, *MNRAS*, 393, 969
 Beaugé, C., Ferraz-Mello, S., & Michtchenko, T. A. 2003, *ApJ*, 593, 1124
 Brahm, R., Jordán, A., & Espinoza, N. 2017a, *PASP*, 129, 034002
 Brahm, R., Jordán, A., Hartman, J., & Bakos, G. 2017b, *MNRAS*, 467, 971
 Bressan, A., Marigo, P., Girardi, L., et al. 2012, *MNRAS*, 427, 127
 Butler, R. P., Marcy, G. W., Williams, E., et al. 1996, *PASP*, 108, 500
 Butler, R. P., Vogt, S. S., Laughlin, G., et al. 2017, *AJ*, 153, 208
 Castelli, F., & Kurucz, R. L. 2004, arXiv:astro-ph/0405087
 Duncan, M. J., Levison, H. F., & Lee, M. H. 1998, *AJ*, 116, 2067
 ESA 1997, ESA SP-1200, The Hipparcos and Tycho Catalogues (Noordwijk: ESA)
 Foreman-Mackey, D., Hogg, D. W., Lang, D., & Goodman, J. 2013, *PASP*, 125, 306
 Gaia Collaboration, Brown, A. G. A., Vallenari, A., et al. 2018, *A&A*, 616, A1
 Gaia Collaboration, Prusti, T., de Bruijne, J. H. J., et al. 2016, *A&A*, 595, A1
 Giguere, M. J., Fischer, D. A., Payne, M. J., et al. 2015, *ApJ*, 799, 89
 Goldreich, P., & Schlichting, H. E. 2014, *AJ*, 147, 32
 Gontcharov, G. A., & Mosenkov, A. V. 2018, *MNRAS*, 472, 3805
 Ida, S., Guillot, T., & Morbidelli, A. 2016, *A&A*, 591, A72
 Johnson, J. A., Payne, M., Howard, A. W., et al. 2011, *AJ*, 141, 16
 Kjeldsen, H., & Bedding, T. R. 2011, *A&A*, 529, L8
 Lee, M. H., & Peale, S. J. 2002, *ApJ*, 567, 596
 Lee, M. H., & Peale, S. J. 2003, *ApJ*, 592, 1201
 Lin, D. N. C., & Papaloizou, J. 1986, *ApJ*, 309, 846
 Lubow, S. H., & D'Angelo, G. 2006, *ApJ*, 641, 526
 Marcy, G. W., & Butler, R. P. 1992, *PASP*, 104, 270
 Marshall, J. P., Wittenmyer, R. A., Horner, J., et al. 2019, *AJ*, 157, 1
 Masset, F., & Snellgrove, M. 2001, *MNRAS*, 320, L55
 Masset, F. S., & Papaloizou, J. C. B. 2003, *ApJ*, 588, 494
 Meschiari, S., Wolf, A. S., Rivera, E., et al. 2009, *PASP*, 121, 1016
 Nelder, J. A., & Mead, R. 1965, *CompJ*, 7, 308
 Nelson, B. E., Robertson, P. M., Payne, M. J., et al. 2016, *MNRAS*, 455, 2484
 Pierens, A., Raymond, S. N., Nesvorný, D., & Morbidelli, A. 2014, *ApJL*, 795, L11

- Pojmanski, G., Pilecki, B., & Szczygiel, D. 2005, *AcA*, **55**, 275
- Press, W. H., Teukolsky, S. A., Vetterling, W. T., & Flannery, B. P. 1992, *Numerical Recipes in FORTRAN. The Art of Scientific Computing* (Cambridge: Cambridge Univ. Press)
- Quirrenbach, A., Reffert, S., & Bergmann, C. 2011, in *AIP Conf. Ser.* 1331, *Planetary Systems beyond the Main Sequence*, ed. S. Schuh, H. Drechsel, & U. Heber (Melville, NY: AIP), 102
- Quirrenbach, A., Trifonov, T., Lee, M. H., & Reffert, S. 2019, *A&A*, in press
- Rein, H., Payne, M. J., Veras, D., & Ford, E. B. 2012, *MNRAS*, **426**, 187
- Rivera, E. J., Laughlin, G., Butler, R. P., et al. 2010, *ApJ*, **719**, 890
- Robinson, S. E., Laughlin, G., Vogt, S. S., et al. 2007, *ApJ*, **670**, 1391
- Robitaille, T. P., Whitney, B. A., Indebetouw, R., & Wood, K. 2007, *ApJS*, **169**, 328
- Sato, B., Omiya, M., Harakawa, H., et al. 2012, *PASJ*, **64**, 135
- Sato, B., Wang, L., Liu, Y.-J., et al. 2016, *ApJ*, **819**, 59
- Stock, S., Reffert, S., & Quirrenbach, A. 2018, *A&A*, **616**, A33
- Tadeu dos Santos, M., Correa-Otto, J. A., Michtchenko, T. A., & Ferraz-Mello, S. 2015, *A&A*, **573**, A94
- Tan, X., Payne, M. J., Lee, M. H., et al. 2013, *ApJ*, **777**, 101
- Trifonov, T., Lee, M. H., Reffert, S., & Quirrenbach, A. 2018, *AJ*, **155**, 174
- Trifonov, T., Reffert, S., Tan, X., Lee, M. H., & Quirrenbach, A. 2014, *A&A*, **568**, A64
- Valenti, J. A., Butler, R. P., & Marcy, G. W. 1995, *PASP*, **107**, 966
- VanderPlas, J., Connolly, A. J., Ivezić, Z., & Gray, A. 2012, in *Proc. Conf. on Intelligent Data Understanding*, ed. K. Das et al. (Hoboken, NJ: IEEE), 47
- Vogt, S. S., Allen, S. L., Bigelow, B. C., et al. 1994, *Proc. SPIE*, **2198**, 362
- Walsh, K. J., Morbidelli, A., Raymond, S. N., O'Brien, D. P., & Mandell, A. M. 2011, *Natur*, **475**, 206
- Wittenmyer, R. A., Horner, J., & Tinney, C. G. 2012, *ApJ*, **761**, 165
- Wittenmyer, R. A., Johnson, J. A., Butler, R. P., et al. 2016, *ApJ*, **818**, 35
- Worthey, G., & Lee, H.-C. 2011, *ApJS*, **193**, 1
- Zechmeister, M., & Kürster, M. 2009, *A&A*, **496**, 577